Phase Control and In-situ Passivation of Quasi-2D Metal Halide Perovskites for Spectrally Stable Blue Light-Emitting Diodes

*Michael Worku[1], Qingquan He[2], Liang-jin Xu[2], Jisook Hong[3], Ruo Xi Yang[3], Liang Tan[*3], Biwu Ma[*1,2]*

[1]Materials Science and Engineering Program, Florida State University, Tallahassee, FL 32306, USA.

[2]Department of Chemistry and Biochemistry, Florida State University, Tallahassee, FL 32306, USA.

[3]The Molecular Foundry, Lawrence Berkeley National Laboratory, Berkeley, CA 94720, USA

Corresponding authors

[*]lztan@lbl.gov

[*]bma@fsu.edu

ABSTRACT

Fabricating efficient and spectrally stable pure-blue perovskite light-emitting diodes (LEDs) has been elusive and remains of great interest. Herein, we show the incorporation of diammonium salts in quasi-2D perovskite precursors for phase control of multiple quantum well structures to yield tunable and efficient emissions in the blue region. With detailed characterizations and computational studies, we discovered the in-situ passivation role played by the diammonium salts, which can effectively modify the surface energies of quasi-2D phases and inhibit the growth of low-bandgap quasi-2D and 3D phases. Such phase control and in-situ passivation could afford blue light-emitting perovskite thin films with high photoluminescence quantum efficiencies (PLQEs), for instance 75 % for the one with emission peaked at 471 nm. Using this perovskite thin film as emitting layer, spectrally stable pure-blue LEDs with an emission peak at 474 nm and a full-width-half-maxima (FWHM) of 26 nm could be fabricated to exhibit a brightness of 290 cd m^{-2} at 8 V and an external quantum efficiency of 2.17 %.

TOC GRAPHICS

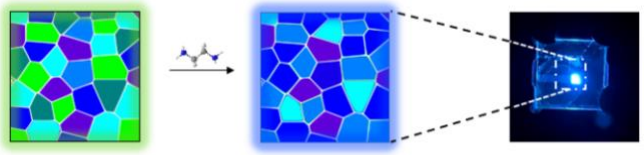

Keywords: Quasi-2D perovskites, blue LEDs, phase control, surface passivation

Introduction

Perovskite light-emitting diodes (PeLEDs) have become potential alternatives to organic and quantum dot LEDs because of their narrow emissions, tunable colors, and facile preparation.[1-2] Green,[3] red,[4] and near-infrared[5-7] PeLEDs have recently been demonstrated with external quantum efficiencies approaching the theoretical maxima. However, fabricating comparatively efficient blue PeLEDs has been more challenging. The difficulty in achieving highly efficient blue PeLEDs stems from the lack of efficient blue emitting perovskite thin films, as well as suitable device architectures.[8] The most popular strategies, thus far, to achieve blue emitting perovskites have been through the use of mixed halide systems,[9-10] quantum dots,[11] or low-dimensional structures, in particular quasi-2D perovskite quantum wells.[12-14] More recently, a combination of quasi-2D perovskites and perovskite quantum dots was also used to fabricate blue PeLEDs.[15] While achieving blue emissions is straightforward for mixed halide perovskites, fast ion migration and phase separation under photo and electrical stresses would easily lead to spectral instability.[16-18] On the other hand, strongly quantum confined blue emitting perovskite nanocrystals have been demonstrated with high PLQEs. However their synthesis and device integration are nontrivial.[19] Similarly, although quasi-2D perovskites hold great promise for color tunable emissions, the difficulty in producing pure phase or phase-controlled multiple quantum well thin films presents a challenge for their application in blue PeLEDs.[20]

Recently, Sargent's group demonstrated an effective approach to controlling the quantum well structures in quasi-2D perovskite thin films by using mixed organic cations (phenethylammonium and isopropylammonium), which afforded narrow emissions from intermediate phases.[21] It was suggested that change in the formation energies of the different phases is responsible for the greatly reduced number of 2D and 3D phases. Similarly, Liao et al. used a mixture of two quasi-2D

perovskite templating organic salts, 1,4-Bis(aminomethyl)benzene bromide ($PDABr_2$) in combination with phenethylammonium bromide (PEABr), to produce deep-blue emitting PeLEDs.[22] It was proposed that the enhanced interaction between $PDABr_2$ and the perovskite surface led to phase modulation in the quasi-2D perovskite thin films. In a second work, the same group used quasi-2D non-templating organic salt N-(2-Bromoethyl)-1,3-propanediamine dihydrobromide along with phenethyl ammonium bromide (PEABr) to obtain sky-blue emitting perovskite thin films.[23] However, the emission peak position and the low PLQEs were less than ideal for wide color gamut display applications. Moreover, the phase control mechanism was never reported. While these recent efforts show the effectiveness of phase controlling using mixed organic cations, there is not a general guideline for the selection of organic cations yet and developing effective quasi-2D phase control routes to achieve efficient blue emissions remains of great interest. Furthermore, the lack of efficient and spectrally stable pure-blue (with emission peaks between 465 nm - 475 nm) thin films and PeLEDs continues to hinder PeLEDs' potential application for wide color gamut displays.

Here we present a facile and effective approach of phase composition control for quasi-2D perovskite thin films with efficient and tunable blue emissions, by using diammonium salts to realize in-situ passivation of quasi-2D phases. We found that the interaction of the nitrogen atoms on the diamine with under-coordinated Pb^{2+} ions on quasi-2D perovskite surfaces through lone-pair donation could effectively change the formation energies of various phases and inhibit the growth of low-bandgap phases. By taking advantage of this facile phase control, we have prepared blue emitting perovskite thin films with tunable emissions from 490 nm to 454 nm, which exhibit high photoluminescence quantum efficiencies (PLQEs) of up to 75 %. We have also fabricated

efficient and spectrally stable blue PeLEDs, as proof of concept, with a maximum EQE of 2.17 % for the device with emission peaked at 474 nm.

Results and Discussion

Quasi-2D perovskite thin films were prepared by substituting varying amounts of CsBr by ethyldiammonium bromide ($EDABr_2$), while keeping the concentration and ratio of PEABr and $PbBr_2$ the same at 1:1. Thin films were prepared using an anti-solvent assisted crystallization technique for the purpose of nanocrystal pinning. Particularly, 500 µl of chloroform was introduced at ~ 28 seconds after the spin cycle began (Figure 1a). The anti-solvent dropping time was optimized to achieve desired crystallinity, film morphology, and optical properties (Figure S1). This preparation technique yielded bright light-emitting thin films without the need for thermal annealing. X-ray diffractograms of three samples with 0 %, 10 % and 20 % $EDABr_2$ substitution show similar diffraction peaks, suggesting the introduction of $EDABr_2$ had little-to-no effect on the crystal structure of the thin films (Figure 1b). The absence of diffraction peak shift confirms that the incorporation of $EDABr_2$ did not lead to the formation of hollow 3D perovskites as with the case of neat $CsPbBr_3$.[24] Moreover, the good crystallinity of the thin films is evidenced by the strong diffraction peaks corresponding to orthorhombic $CsPbBr_3$ and <n> = 3 quasi-2D phases for all cases.[25-26] Crystallite size analysis of the XRD patterns reveals that the average crystallite size ranges from 8 to 12 nm. However, the 10 % sample showed an intense diffraction peak at $2\theta \approx 38°$ corresponding to the (123) lattice plane of the orthorhombic $CsPbBr_3$ phase. This peak implies the preferential in-plane orientation of the thicker emitting quasi-2D phases in the 10 % sample. In addition, the prepared thin films displayed good film morphology, which is further enhanced with the substitution of $EDABr_2$. As shown in Figure 1c, the root-mean-square roughness

(RMS) of the thin films decreased from 5.4 nm for the control sample to 0.7 nm and 1.5 nm for the 10 % and 20 % substituted films, respectively.

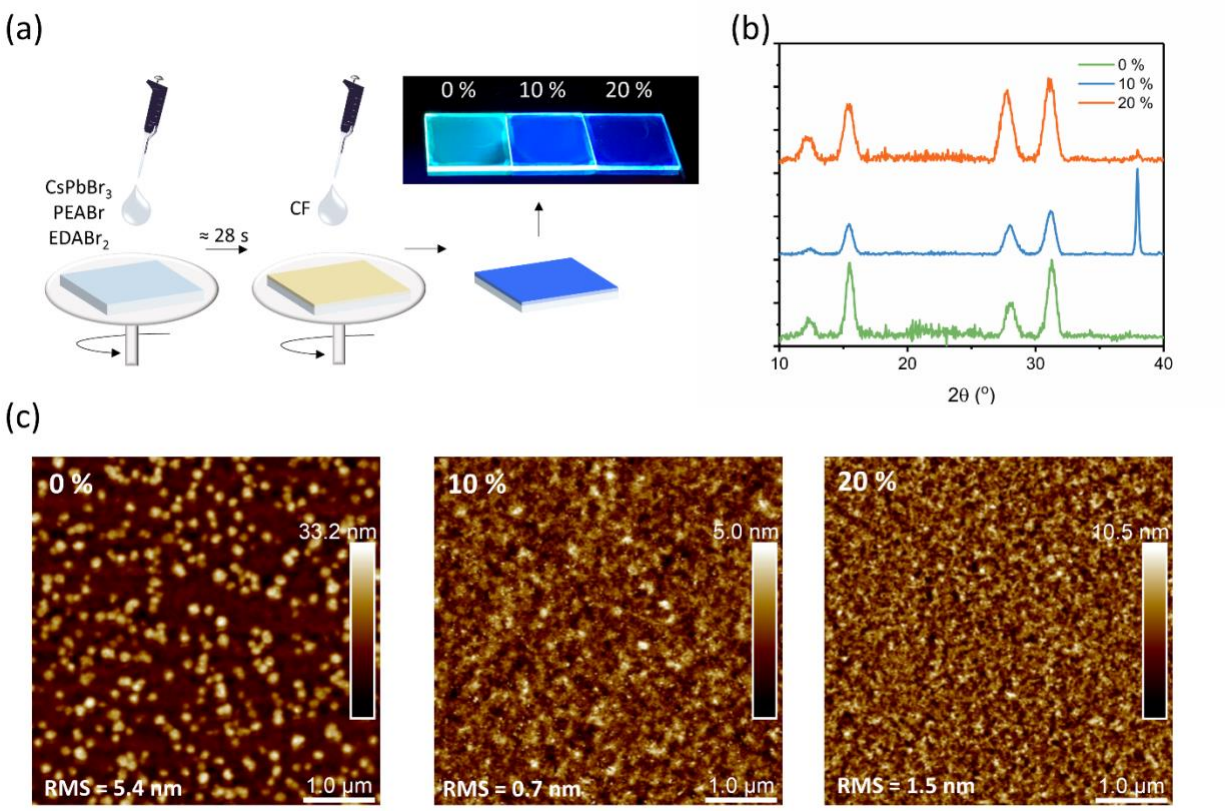

Figure 1. (a) Schematic showing the anti-solvent assisted spin coating used to prepare thin films; inset shows the thin films with 0 %, 10 % and 20 % $EDABr_2$ substituted for CsBr under UV irradiation; (b) X-ray diffraction patterns of thin films; (c) Atomic force microscopic images of thin films.

The quasi-2D nature of the perovskite thin films was confirmed via UV-Vis absorption spectra, which showed distinct excitonic absorption peaks for n = 1, 2 and 3 phases (Figure 2a). For the control sample without $EDABr_2$ substitution, large thickness and low-bandgap phases (n > 10) were also present, as evidenced by the broad absorption band extending up to 500 nm. However,

the broad absorption band edge was blue shifted for 10 % and 20 % $EDABr_2$ substituted samples, suggesting the absence of low-bandgap phases. As reported previously, the emission from multiple quantum well thin films is often ascribed to the phases with the lowest bandgaps, as a result of fast energy/charge funneling.[20] In our samples, we observed similar emission characteristics from the phases with the lowest bandgaps. The emission peak blue shifted from 490 nm for the control sample with no substitution to 471 nm and 454 nm for 10 % and 20 % $EDABr_2$ substituted thin films, respectively (Figure 2b). This shift is indicative of the progressive reduction of low-bandgap quasi-2D and 3D phases upon the incorporation of $EDABr_2$. The full-width-half-maxima (FWHM) of the emissions were found to be 28 nm, 28 nm, and 29 nm for 0 %, 10 %, and 20 % $EDABr_2$ substituted thin films, respectively, further confirming the emissions to be from a cluster of the lowest bandgap phases.

Time-resolved photoluminescence (TRPL) experiments showed tri-exponential decay behaviors for all prepared samples, suggesting the presence of multiple recombination pathways that can be ascribed to a cluster of emitting phases. $EDABr_2$ substitution led to increased average PL decay lifetimes from 40 ns for the control sample to 72 ns and 92 ns for 10 % and 20 % $EDABr_2$ substituted samples, respectively (Figure 2c). It can be inferred from this result that in addition to emission and phase composition control, $EDABr_2$ substitution could also provide surface trap/defect passivation. This surface passivation was further supported by PLQE measurements that showed an increase from 55 % for the control sample to 75 % for the 10 % substituted thin film. Further increase to 20 % substitution resulted in a decline of PLQE to 40 %, which could be attributed to deep traps within the relatively wide bandgap phases responsible for the emission.[20, 27] Although an increased PL decay lifetime was observed for the 20 % substituted thin film, a lower PLQE was recorded as compared to that of 10 % substituted thin films. We attribute this

incongruency to the differing emitting species in the 10 % and 20 % substituted thin films that display distinct PL decay kinetics. The peak wavelength and the corresponding PLQEs for the three samples are summarized in Figure 2d.

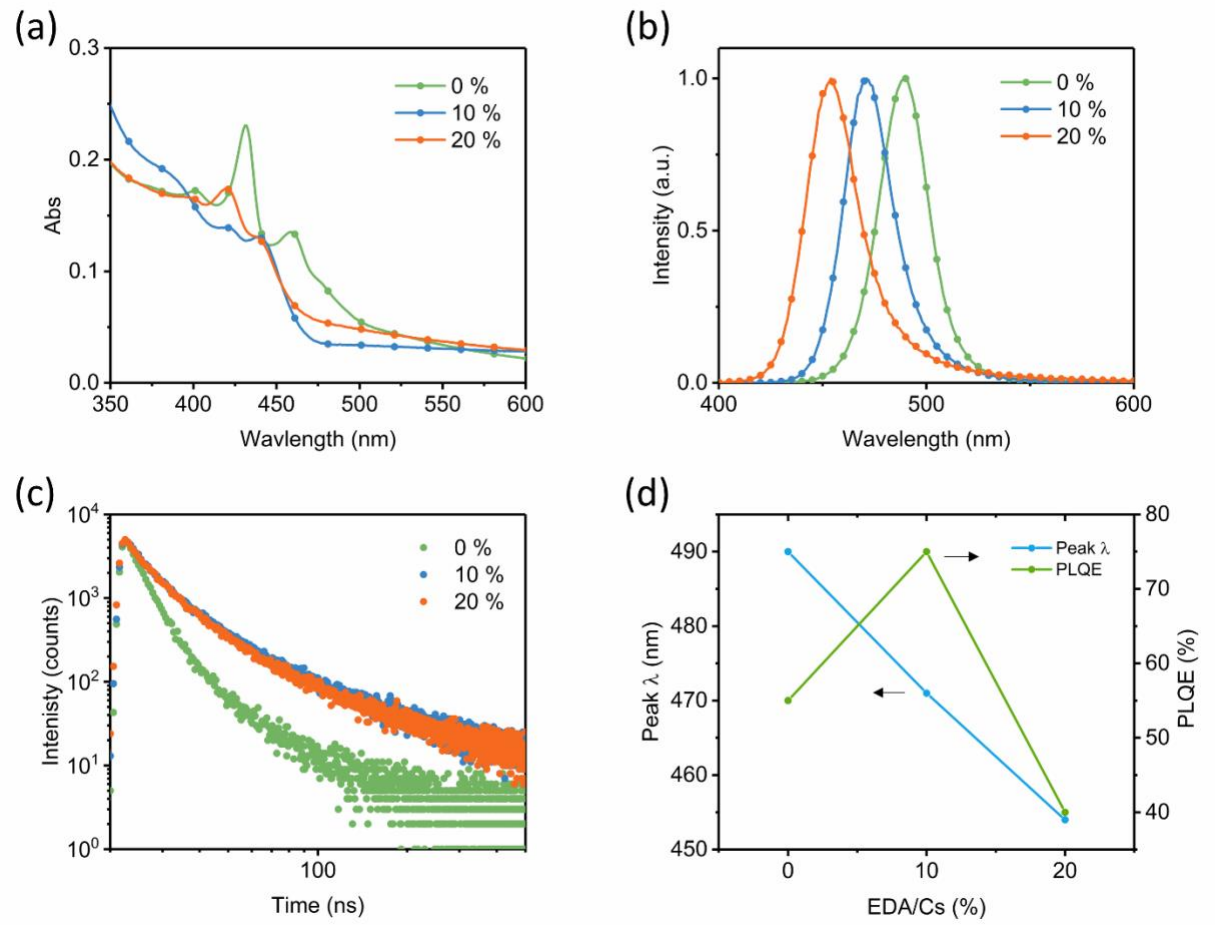

Figure 2. (a) UV-vis absorption spectra, (b) photoluminescence emission spectra, (c) time-resolved photoluminescence, and (d) peak wavelength and photoluminescence quantum efficiency of thin films with 0 %, 10 % and 20 % $EDABr_2$ substituted for CsBr.

The defect passivation of perovskites by EDA has previously been investigated in $MAPbBr_3$ by Lee et al., where the nitrogen atoms on EDA bonded to undercoordinated Pb^{2+} ions to reduce trap assisted non-radiative recombination.[28] Here we hypothesize a similar passivation scheme, in

which EDA attaches to the surface of quasi-2D phases to passivate surface trap sites. Unlike surface passivation through post-treatment, the presence of $EDABr_2$ in the precursor enables in-situ passivation during nucleation and crystal growth. Fourier transform infrared spectroscopy (FT-IR) was performed on neat $EDABr_2$ films and $EDABr_2$ substituted quasi-2D thin films to reveal the effects of $EDABr_2$ incorporation on the formation of quasi-2D perovskite thin films. As shown in Figure 3a, both N-H (ν(N-H)) and C-H (ν(C-H)) stretching bands shift to higher frequencies, suggesting bond length reduction or change in electronegativity of neighboring atoms. Moreover, the N-H scissoring band (δ (N-H)) shifts from 1592 cm^{-1} for the neat $EDABr_2$ sample to 1586 cm^{-1} and 1585 cm^{-1} for 10 % and 20 % substituted thin films. This shift implies the inhibition of the scissoring vibration because of interactions with the metal halide surfaces. These results suggest that EDA interacts with the perovskite surfaces through either hydrogen bonding or lone pair donation from the nitrogen atom to under-coordinated Pb^{2+} cations to form Lewis acid-base complexes.

To further explore the nature of the interactions between EDA and the metal halide surfaces, X-ray photoelectron spectroscopy (XPS) was conducted on the control and in-situ passivated thin films. As illustrated in Figure 3b, the C 1s photoelectron spectra were resolved into two gaussian spectra corresponding to C-C and C-N bonding. We observe steady shifts of the C-N spectra to higher binding energies from a peak of 285.8 eV for the control sample to 285.96 eV and 286.31 eV for samples with 10 % and 20 % $EDABr_2$ substitutions, respectively. This shift is indicative of shortening of the C-N bond or increased interaction between nitrogen atoms and their carbon neighbors, likely caused by a change in the electronegativity of the nitrogen atoms. Because a change in the C-N bond characteristics is not expected in the case of hydrogen bonding, we attribute the binding energy shift to the removal of the lone pair from the nitrogen atom in EDA.

This lone pair removal would lead to a stronger interaction between the nitrogen atom and the neighboring carbon atom. The formation of a dative covalent bond between Lewis base amines and the Lewis acid Pb^{2+} through lone pair donation was recently investigated by Rand and colleagues.[29] Thus, we believe that a similar dative covalent bonding between EDA and under-coordinated Pb^{2+} could be responsible for the in-situ passivation. However, the cause for deprotonation of EDA^{2+} remains unclear. Photoelectron spectra of Pb 4f and Br 3d do not show appreciable changes compared to the control sample (Figure S2).

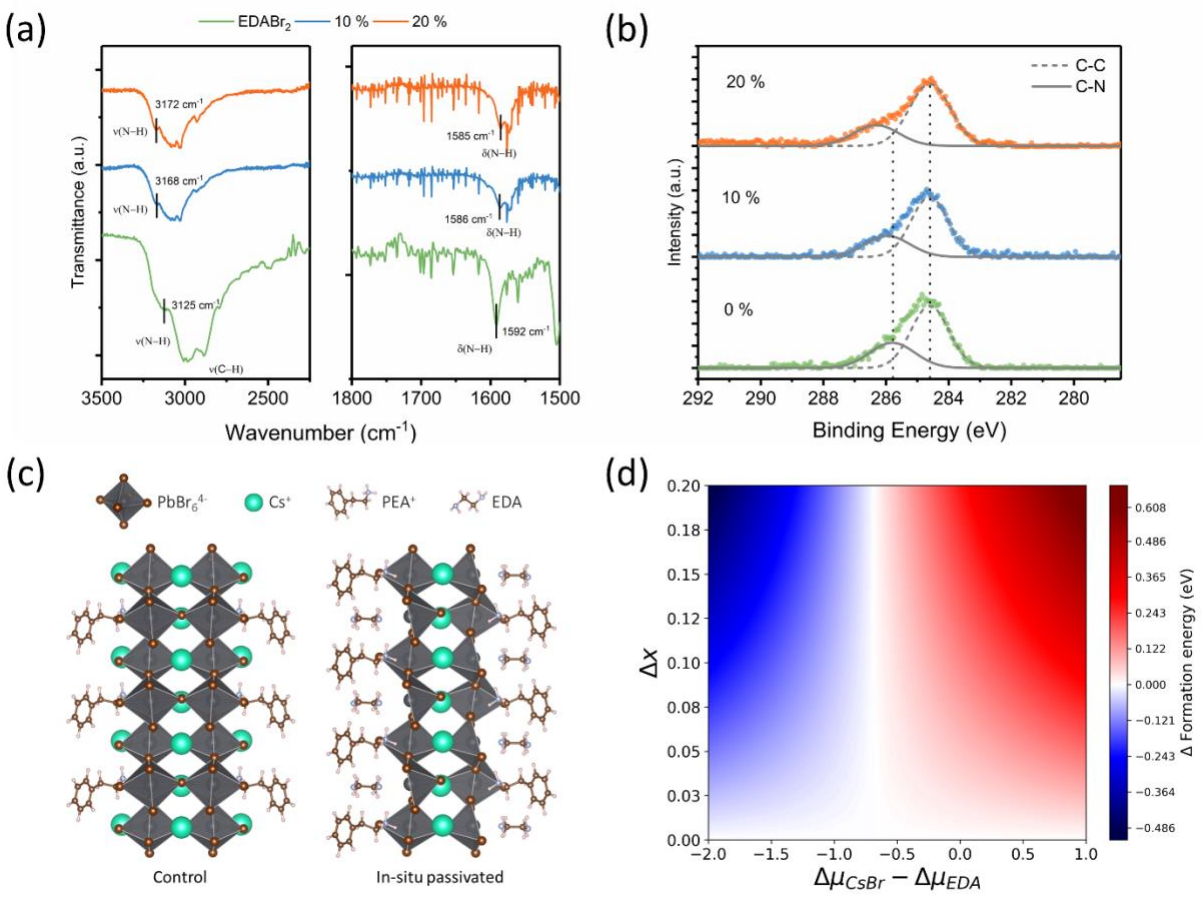

Figure 3. (a) Fourier transform infrared absorption spectra of thin films (ν(N-H) and ν(C-H) refer to N-H and C-H bond stretching, respectively; δ(N-H) refers to N-H scissoring) (b) C 1s

photoelectron spectra of thin films; (c) Optimized structures of control and in-situ passivated quasi-2D (n = 2) phases; (d) Calculated surface formation energy of in-situ passivated n=2 surface compared to control unsubstituted surface, as a function of $EDABr_2$ substitution (Δx) and chemical potentials ($\Delta\mu_{CsBr} - \Delta\mu_{EDA}$). The blue region indicates the relative stability of a partially EDA-substituted phase over the unsubstituted phase can be achieved by choosing higher Δx and smaller $\Delta\mu_{CsBr} - \Delta\mu_{EDA}$, which corresponds to higher concentration of EDA and lower concentration of CsBr.

To gain a better understanding of the in-situ passivation by EDA, density functional theory (DFT) calculations were carried out to obtain optimized structures of the control and surface passivated n = 2 quasi-2D phases (Figure 3c). In these structures, the C-N bond length of in-situ passivated phase is shortened by 1.07 % (1.479 Å) compared to that of control phase with only PEA^+ (1.495 Å), confirming that lone pair donation leads to shortened C-N bonds in these systems. In comparison, an alternative bonding configuration where the amino group of EDA^{2+} forms hydrogen bonds to Br^- was found to have longer C-N bonds of 1.495 Å and is therefore unlikely here. We also investigated the surface energies of control and in-situ passivated phases, finding stable formation of partially $EDABr_2$ substituted surfaces when EDA chemical potentials are sufficiently high compared to CsBr (Figure 3d). These results indicate the partial substitution of CsBr by $EDABr_2$ leads to the preferential formation of wide band gap quasi-2D phases and inhibits growth of low band gap quasi-2D and 3D phase. The DFT computed band gap of the $EDABr_2$ substituted phase was also found to be larger than that of the control phase by 0.10 eV. While excitonic effects are not included in these calculations, they show that part of the blue shift observed in the experiment is a result of EDA bonding to optically active Pb orbitals.

To investigate whether EDA molecules can accomplish the same feat as $EDABr_2$ salt, we introduced 10 mol % of EDA into the quasi-2D precursor solution. As can be observed from Supplementary figure S2, the narrow and strongly blue-shifted emission is evidence that diamine molecules can, indeed, attach to the perovskite surface and effect phase control. However, the emission intensity and PL decay lifetime do not indicate significant defect passivation as seen with quasi-2D thin films containing $EDABr_2$. This is indicative of the role played by the Br^- in the diammonium salt in passivating surface and vacancy defects to improve the emission property. Thus, the use of the diammonium salt instead of the diamine not only accomplishes effective phase control but also surface defect passivation for improved optical properties.

To test the universality of in-situ passivation and phase control by diammonium salts, we replaced $EDABr_2$ with N-methylethyldiammonium bromide (N-$MEDABr_2$) and dimethylethyldiammonium bromide ($DMEDABr_2$). As shown in supplementary Figures S4 and S5, perovskite thin films containing the two new diammonium salts exhibit similar photophysical characteristics as those with $EDABr_2$ substitution. Emission peaks and absorption band edges blue-shift with increased substitution, for both cases. However, the extent of emission tuning was limited, because the band gap of $DMEDABr_2$ substituted phase showed less significant enhancement in band gap, with its DFT gap calculated to be 1.68 eV, a 0.06 eV enhancement over the control phase (1.62 eV), which is less than the $EDABr_2$ substituted phase. In addition, the average PL decay lifetimes also increased for both systems with N-$MEDABr_2$ and $DMEDABr_2$ substitutions, indicating certain degrees of surface trap/defect passivation.

Considering the high PLQEs, tunable emissions, and good film morphology, these quasi-2D perovskite thin films could be promising candidates for blue PeLEDs. We fabricated standard p-i-n devices with PEDOT:PSS (poly(3,4-ethylenedioxythiophene) polystyrene sulfonate) as hole

injection layer, TPBi (2,2′,2"-(1,3,5-Benzinetriyl)-tris(1-phenyl-1-H-benzimidazole) as electron transport layer, and LiF (lithium fluoride) as electron injection buffer (Figure 4a). The thin films displayed similar emission intensities on PEDOT:PSS, confirmed by the PL decay as shown in Figure S6. Devices based on 10 % substituted thin films displayed a strong blue emission centered at 474 nm with a FWHM of 26 nm (Figure 4b). The devices showed a peak luminance of 290 cd m^{-2} at 8 V (Figure 4c) and a turn-on voltage of 4.1 V. A maximum external quantum efficiency (EQE) of 2.17 % and a current efficiency of 1.95 cd A^{-1} were recorded (Figure 4d). The devices also showed exceptional spectral stability under varying bias, where the emission peak did not show any change when the operation voltage was successively increased from 5 V to 9 V (Figure 4e). Operating the device under 5.4 V for 5 minutes also did not result in any shift of electroluminescence (Figure 4f). The half-lifetime (T_{50}) of the device measured at an initial luminance of 20 cd/m^2 was found to be 150 s, as shown in Figure S7a. The chromaticity coordinates were close to those specified by Recommendation BT.2020 for blue LEDs (Figure S7b). EQE statistics show a gaussian distribution with an average EQE of 1.74 % and a standard deviation of 0.29 %, indicating the good reproducibility of the devices (Figure S7c). These devices represent one of only few pure bromide based blue PeLEDs reported to date with emissions in the pure-blue region and EQEs exceeding 1 % (Table S1). Similarly, spectrally stable LEDs with emissions peaked at 495 nm and 463 nm were also fabricated using the control and 20 % substituted perovskite thin films, which exhibit maximum EQEs of 1.2 % and 0.24 %, respectively (Figures S8 and S9).

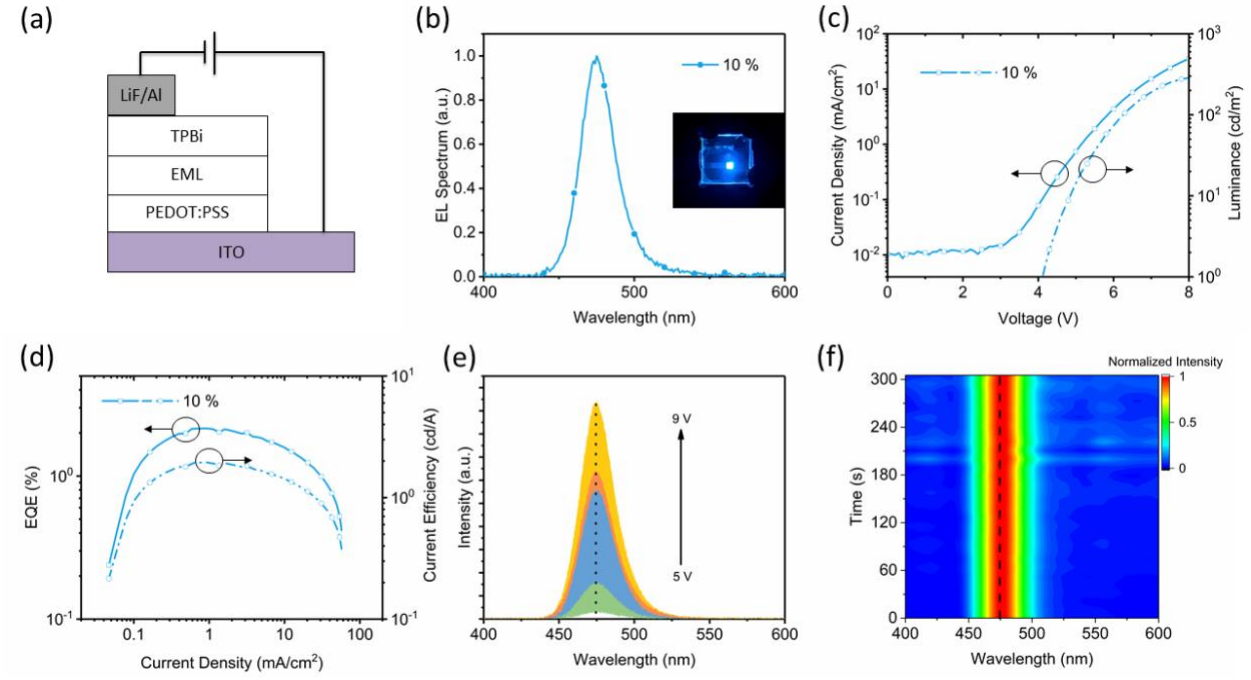

Figure 4. (a) Device architecture used in this study; (b) Electroluminescence (EL) spectrum of 10 % substituted device; inset: photo of 10 % device under operation. (c) Current density and luminance versus voltage, (d) External quantum efficiency (EQE) and current efficiency versus current density for 10 % device; (e) Spectral stability of 10 % device under varying bias (f) Spectral stability of 10 % device under continuous operation at 5.4 V.

We also fabricated devices based on the bulkier diammonium salts N-MEDABr$_2$ and DMEDABr$_2$, which showed blue and sky-blue emissions centered at 481 nm and 487 nm (Figure S10), respectively. Interestingly, devices based on DMEDABr$_2$ showed higher maximum luminance and EQE as compared to those based on N-MEDBr$_2$. This improvement is likely due to easier charge injection into the relatively lower bandgap emitting phases of DMEDA based devices as compared to N-MEDA devices. We hypothesized poor charge balance to be the cause for the modest performance shown here. Single-carrier devices were fabricated to study the hole and electron currents in the 10 % EDABr$_2$ substituted devices. As shown in Figure S11, the hole current is more

than an order of magnitude higher than the electron current. Thus, we believe device engineering to achieve good charge balance will be necessary to improve the device performance and stability of these blue LEDs. Moreover, manipulating the orientation of quasi-2D phases with high aspect ratio could lead to increased light extraction efficiency, which can translate improved device performance.[30]

Conclusion

In summary, we have established an effective approach of phase control for quasi-2D cesium lead bromide perovskite thin films to achieve efficient blue emissions. The use of various diammonium salts, for instance $EDABr_2$, can not only reduce the number of quantum well structures in quasi-2D perovskite thin films to obtain narrow emissions, but also effectively passivate the quasi-2D surfaces to enhance the photoluminescence quantum efficiency. The composition and property tuning were found to be results of modified surface energies of the in-situ surface passivated quasi-2D phases, which in turn inhibits the growth of low bandgap quasi-2D and 3D phases. The findings of this study not only indicate the role of diammonium salts in quasi-2D perovskite phase distribution control but also that the described Lewis acid-base interaction mechanism can be leveraged with other Lewis base systems to achieve the same feat. Moreover, spectrally stable pure blue LEDs have been fabricated using these multiple quantum well perovskite thin films with engineered phases. These devices represent one of the highest efficiencies for pure-bromide and pure-blue PeLEDs with excellent spectral stability. This work enriches our fundamental understanding of the composition and phase control of quasi-2D perovskite thin films with desired photophysical properties, which also paves a new way to achieving spectrally stable and efficient PeLEDs.

Experimental Section

Materials

PbB_2, CsBr, phenethylamine, ethylenediamine, N-methylethylenediamine, dimethylethylenediamine, TPBi, LiF were purchased from Sigma Aldrich. PEDOT:PSS (CH8000) was purchased from Heraeus. $CsPbBr_3$ powder was synthesized following previously reported procedures.[3] PEABr, $EDABr_2$, N-$MEDABr_2$ and $DEMEDABr_2$ were synthesized by mixing with equivalent amounts of HBr in an ethanol medium and drying the obtained white precipitate overnight under vacuum.

Thin film preparation

For the control sample, 1:1 ratio of PEABr and $CsPbBr_3$ were dissolved in DMSO to make a 0.2 M precursor solution. For the 10 % and 20 % substituted samples, corresponding molar amounts of $EDABr_2$ were substituted for CsBr to make 0.2 M precursor solutions. The precursor solution was spin cast at 3000 RPM for 60 s and chloroform was introduced 28 s after the spin cycle began. No annealing was necessary.

Characterization

Absorption spectra were obtained using an Agilent Technologies Cary 5000 UV-Vis-NIR spectrophotometer. Steady-state PL was carried out using an Edinburgh FS5 steady state spectrometer with a 150 W xenon lamp at an excitation wavelength of 365 nm. TRPL was collected using Time Correlated Single Photon Counting (TCSPC) for 10,000 counts. Excitation was provided by an Edinburgh EPL-360 picosecond pulsed diode laser. The PL decay was fit using a tri-exponential decay function. The average lifetime was obtained from the tri-exponential decays according to equation 1.

$$\tau_{ave} = \Sigma\alpha_i\tau_i^2/\Sigma\alpha_i\tau_i,\ i = 1, 2, 3 \quad (1)$$

where τ_i represents the decay time and α_i represents the amplitude of each component. PLQE measurements were performed in accordance to what has been reported previously.[31] Briefly, a Hamamatsu Quantaurus-QY Spectrometer (Model C11347-11) equipped with a xenon lamp, an

integrating sphere sample chamber and a CCD detector. The PLQEs were calculated by the equation: $\eta QE = \frac{I_S}{E_R - E_S}$, in which $I_s$represents the luminescence emission spectrum of the sample, E_R is the spectrum of the excitation light for the reference (empty substrate) , and E_S is the excitation spectrum for exciting the sample. The PLQE measurements were done consecutively at an excitation wavelength of 340 nm and a power density of 0.3 mW cm^{-2} were used for all samples. XRD patterns were obtained using a Rigaku Smartlab powder diffractometer equipped with a Cu Kα X-ray source. Diffraction patterns were recorded from 10° to 40° 2θ with a step size of 0.05° under a tube current of 30 mA and tube voltage of 40 KV. To determine crystallite sizes from XRD patterns, the Halder-Wagner method, as implemented in the Rigaku Smartlab Studio II software, was used. Briefly, the diffraction peaks were fit using a pseudo-Voigt function and the Halder-Wagner equation $\frac{\beta^2}{tan^2\theta} = \frac{K\lambda}{L} \cdot \frac{\beta}{tan\,\theta \sin\theta} + 16e^2$, where β is the integral linewidth, θ the diffraction angle, λ the x-ray wavelength, K the Scherer constant taken as 1, L the crystallite size and e the lattice strain, was linearly fit to estimate the crystallite size of the thin films.[32] A Si standard was used to account for instrumental broadening. XPS was conducted using a PHI 5000 series XPS equipped with a dual anode x-ray source. For our purpose, Al Kα radiation with a photon energy of 1486.6 eV at a take-off angle of 45° and a pass energy of 35.75 eV were used. Charge compensation was performed using adventitious C 1s peak (284.6 eV). Spectra background were fit and subtracted using an integrated Shirley function. XPS curves were deconvoluted using a Voight peak function for metal core electron spectra and gaussian peak functions for the rest. FTIR was performed using an ATR accessory on a JASCO FT-IR 6800 spectrometer. Thin films were spun cast on quartz substrate for this experiment. AFM images were taken on a Bruker Icon scanning probe microscope in tapping mode.

DFT calculation

The calculations were performed using Vienna *Ab-initio* Simulation Package (VASP)[33-34] which is based on projector-augmented-plane-wave method with Perdew-Burke-Ernzerhof revised for solids (PBEsol) exchange-correlation functional.[35] Spin-orbit coupling was not used in optimization calculations, and was included in band gap calculations. We adopted the cell parameters for $CsPbBr_3$[36] and fully relaxed the atomic positions until force between atoms become less than 0.001 eV $Å^{-1}$ using the energy cutoff of 400 eV and 5x5x1 mesh for k-point sampling.

The formation energy of an EDA-substituted surface can be written as:

$$FE = E[Cs_2Pb_4Br_{12})_2(PEA)_2(CsBr)_{2(1-x)}EDA_{2x}] - 4E[CsPbBr_3] - (-2x\mu_{CsBr} + 2\mu_{PEABr} + 2x\mu_{EDA}) \quad (2)$$

where E is the DFT total energy of a compound, and μ stands for the chemical potential, e.g. $\mu_{CsBr} = E[CsBr] + \Delta\mu_{CsBr}$. The chemical potential depends on the synthesis condition, therefore $\Delta\mu$ can be tuned by tuning the concentration of the reactants.

To compare phase stability of partially substituted and unsubstituted slabs, we calculate the difference in the formation energies:

$$\mathrm{FE}(x > 0) - \mathrm{FE}(x = 0) = xE[(Cs_2Pb_4Br_{12})_2(PEA)_2EDA_2] - xE[(Cs_2Pb_4Br_{12})_2(PEA)_2(CsBr)_2] - 2xE[EDA] + 2xE[CsBr] + 2x(\Delta\mu_{CsBr} - \Delta\mu_{EDA}) \quad (3)$$

Device fabrication

ITO-coated glass substrates were cleaned by successive sonication in detergent solution, deionized water, acetone, and isopropanol for 15 min at 40 °C and UV ozone cleaned for 20 mins. PEDOT:PSS was spun-cast onto the cleaned ITO coated glass substrate at 4500 rpm for 45s and baked at 150 °C for 20 min to obtain a 30 nm thin film. A perovskite precursor solution of 0.2 M

concentration was spin coated on the top at 3000 rpm for 60 s. 500 µl of anhydrous chloroform was dropped ~ 28 S after the spin cycle began. The thickness of the quasi-2D perovskite films were found to be ~ 50 nm. A 40 nm thick layer of TPBi and 1 nm LiF were successively evaporated at rates of 1.0 Å s^{-1} and 0.1 Å s^{-1}, respectively, under high vacuum (< 3 × 10−6 mbar). Al was then deposited at a rate of 3 Å s^{-1}. The active area was determined by the overlapping area between the ITO and Al strips, which was 4 mm^2. Hole-only and electron-only devices were fabricated using the device architectures ITO/PEDOT:PSS/EML/MoO_x/Al and ITO/SnO_2/EML/TPBi/LiF/Al, respectively. MoO_x was deposited at a rate of 0.3 Å s^{-1} to obtain 10 nm thin films. SnO_2 thin films were prepared by diluting commercial SnO_2 colloidal solution with deionized water at 1:6 ratio and using a two-step spin-coating procedure (500 RPM for 10 s followed by 3000 RPM for 30 s) to obtain a 30 nm thin film. The thin films were immediately annealed at 200 °C for 1 hour.

Device testing

The devices were tested inside of a glovebox after fabrication. The electrical and optical intensity characteristics of the devices were measured with a Keithly 2400 sourcemeter/multimeter coupled to an FDS 1010 Si photodiode (Thor labs). Only light emitted from the front face of the device was collected and used in subsequent efficiency calculations. The electroluminescence (EL) spectra and stability were measured using a USB4000 spectrometer (Ocean Optics). The operational stability test was conducted under constant current density.

ASSOCIATED CONTENT

Supporting Information. Anti-solvent optimization PL, TRPL, XRD, AFM, XPS Survey, Pb 4f and Br 3d photoelectron spectra of thin films, photophysical characterization of EDA, N-MEDABr_2 and DMEDABr_2 substituted quasi-2D thin films, TRPL on ITO/PEDOT:PSS, device

statistics, CIE 1931 plot and lifetime of 10 % devices, device characterization of 0 % and 20 % devices, device characteristics of N-MEDA and DMEDA substituted films, single-carrier device characteristics of 10 % EDA substituted sample.

AUTHOR INFORMATION

Michael Worku – mdw16@my.fsu.edu

Qingquan He – qhe@fsu.edu

Liang-jin Xu – lxu3@fsu.edu

Jisook Hong – jisookhong@lbl.gov

Ruo Xi Yang – ruoxiyang@lbl.gov

*Liang Tan – lztan@lbl.gov

*Biwu Ma – bma@fsu.edu

Notes

The authors declare no competing financial interest.

ACKNOWLEDGEMENT

This work was primarily supported by the National Science Foundation (ECCS-1912911). Partial of the work on the characterizations of photophysical properties and device fabrication was supported by the Air Force Office of Scientific Research (AFOSR) under contract No. FA9550-18-1-0231. J. H, R. X. Y, and L. Z. T. were supported by the Molecular Foundry, a DOE Office of Science User Facility supported by the Office of Science of the U.S. Department of Energy under Contract No. DE-AC02-05CH11231. This research used resources of the National Energy Research Scientific Computing Center, a DOE Office of Science User Facility supported by the

Office of Science of the U.S. Department of Energy under Contract No. DE-AC02-05CH11231. The authors also thank Dr. J.S. Raaj Vellore Winfred for help with FT-IR measurements and Dr. Jingjiao Guan for providing facility use.

REFERENCES

1. Kim, Y. H.; Cho, H.; Lee, T. W., Metal Halide Perovskite Light Emitters. *Proc Natl Acad Sci U S A* **2016,** *113*, 11694-11702.

2. Quan, L. N.; Rand, B. P.; Friend, R. H.; Mhaisalkar, S. G.; Lee, T. W.; Sargent, E. H., Perovskites for Next-Generation Optical Sources. *Chem. Rev.* **2019,** *119*, 7444-7477.

3. Lin, K.; Xing, J.; Quan, L. N.; de Arquer, F. P. G.; Gong, X.; Lu, J.; Xie, L.; Zhao, W.; Zhang, D.; Yan, C.; Li, W.; Liu, X.; Lu, Y.; Kirman, J.; Sargent, E. H.; Xiong, Q.; Wei, Z., Perovskite Light-Emitting Diodes with External Quantum Efficiency Exceeding 20 Per Cent. *Nature* **2018,** *562*, 245-248.

4. Chiba, T.; Hayashi, Y.; Ebe, H.; Hoshi, K.; Sato, J.; Sato, S.; Pu, Y.-J.; Ohisa, S.; Kido, J., Anion-Exchange Red Perovskite Quantum Dots with Ammonium Iodine Salts for Highly Efficient Light-Emitting Devices. *Nat Photonics* **2018,** *12*, 681.

5. Cao, Y.; Wang, N.; Tian, H.; Guo, J.; Wei, Y.; Chen, H.; Miao, Y.; Zou, W.; Pan, K.; He, Y.; Cao, H.; Ke, Y.; Xu, M.; Wang, Y.; Yang, M.; Du, K.; Fu, Z.; Kong, D.; Dai, D.; Jin, Y.; Li, G.; Li, H.; Peng, Q.; Wang, J.; Huang, W., Perovskite Light-Emitting Diodes Based on Spontaneously Formed Submicrometre-Scale Structures. *Nature* **2018,** *562*, 249-253.

6. Zhao, B.; Bai, S.; Kim, V.; Lamboll, R.; Shivanna, R.; Auras, F.; Richter, J. M.; Yang, L.; Dai, L.; Alsari, M., High-Efficiency Perovskite–Polymer Bulk Heterostructure Light-Emitting Diodes. *Nat Photonics* **2018,** *12*, 783.

7. Xu, W.; Hu, Q.; Bai, S.; Bao, C.; Miao, Y.; Yuan, Z.; Borzda, T.; Barker, A. J.; Tyukalova, E.; Hu, Z., Rational Molecular Passivation for High-Performance Perovskite Light-Emitting Diodes. *Nat Photonics* **2019,** *13*, 418.

8. Li, C.-H. A.; Zhou, Z.; Vashishtha, P.; Halpert, J. E., The Future Is Blue (Leds): Why Chemistry Is the Key to Perovskite Displays §. *Chem. Mater.* **2019,** *31*, 6003-6032.

9. Gangishetty, M. K.; Hou, S.; Quan, Q.; Congreve, D. N., Reducing Architecture Limitations for Efficient Blue Perovskite Light-Emitting Diodes. *Adv. Mater.* **2018,** *30*, e1706226.

10. Hou, S.; Gangishetty, M. K.; Quan, Q.; Congreve, D. N., Efficient Blue and White Perovskite Light-Emitting Diodes Via Manganese Doping. *Joule* **2018,** *2*, 2421-2433.

11. Bohn, B. J.; Tong, Y.; Gramlich, M.; Lai, M. L.; Doblinger, M.; Wang, K.; Hoye, R. L. Z.; Muller-Buschbaum, P.; Stranks, S. D.; Urban, A. S.; Polavarapu, L.; Feldmann, J., Boosting Tunable Blue Luminescence of Halide Perovskite Nanoplatelets through Postsynthetic Surface Trap Repair. *Nano Lett.* **2018,** *18*, 5231-5238.

12. Li, Z.; Chen, Z.; Yang, Y.; Xue, Q.; Yip, H. L.; Cao, Y., Modulation of Recombination Zone Position for Quasi-Two-Dimensional Blue Perovskite Light-Emitting Diodes with Efficiency Exceeding 5. *Nat Commun* **2019,** *10*, 1027.

13. Kumar, S.; Jagielski, J.; Yakunin, S.; Rice, P.; Chiu, Y. C.; Wang, M.; Nedelcu, G.; Kim, Y.; Lin, S.; Santos, E. J. G.; Kovalenko, M. V.; Shih, C. J., Efficient Blue Electroluminescence Using Quantum-Confined Two-Dimensional Perovskites. *ACS Nano* **2016,** *10*, 9720-9729.

14. Wang, Q.; Ren, J.; Peng, X. F.; Ji, X. X.; Yang, X. H., Efficient Sky-Blue Perovskite Light-Emitting Devices Based on Ethylammonium Bromide Induced Layered Perovskites. *Acs Appl Mater Inter* **2017,** *9*, 29901-29906.

15. Liu, Y.; Cui, J.; Du, K.; Tian, H.; He, Z.; Zhou, Q.; Yang, Z.; Deng, Y.; Chen, D.; Zuo, X., Efficient Blue Light-Emitting Diodes Based on Quantum-Confined Bromide Perovskite Nanostructures. *Nat Photonics* **2019**, 1-5.

16. Yoon, S. J.; Kuno, M.; Kamat, P. V., Shift Happens. How Halide Ion Defects Influence Photoinduced Segregation in Mixed Halide Perovskites. *ACS Energy Lett* **2017,** *2*, 1507-1514.

17. Vashishtha, P.; Halpert, J. E., Field-Driven Ion Migration and Color Instability in Red-Emitting Mixed Halide Perovskite Nanocrystal Light-Emitting Diodes. *Chem. Mater.* **2017,** *29*, 5965-5973.

18. Zhang, H.; Fu, X.; Tang, Y.; Wang, H.; Zhang, C.; William, W. Y.; Wang, X.; Zhang, Y.; Xiao, M., Phase Segregation Due to Ion Migration in All-Inorganic Mixed-Halide Perovskite Nanocrystals. *Nat Commun* **2019,** *10*, 1-8.

19. Shamsi, J.; Urban, A. S.; Imran, M.; De Trizio, L.; Manna, L., Metal Halide Perovskite Nanocrystals: Synthesis, Post-Synthesis Modifications, and Their Optical Properties. *Chem. Rev.* **2019,** *119*, 3296-3348.

20. Yuan, M.; Quan, L. N.; Comin, R.; Walters, G.; Sabatini, R.; Voznyy, O.; Hoogland, S.; Zhao, Y.; Beauregard, E. M.; Kanjanaboos, P.; Lu, Z.; Kim, D. H.; Sargent, E. H., Perovskite Energy Funnels for Efficient Light-Emitting Diodes. *Nat Nanotechnol* **2016,** *11*, 872-877.

21. Xing, J.; Zhao, Y.; Askerka, M.; Quan, L. N.; Gong, X.; Zhao, W.; Zhao, J.; Tan, H.; Long, G.; Gao, L.; Yang, Z.; Voznyy, O.; Tang, J.; Lu, Z. H.; Xiong, Q.; Sargent, E. H., Color-Stable Highly Luminescent Sky-Blue Perovskite Light-Emitting Diodes. *Nat Commun* **2018,** *9*, 3541.

22. Yuan, S.; Wang, Z. K.; Xiao, L. X.; Zhang, C. F.; Yang, S. Y.; Chen, B. B.; Ge, H. T.; Tian, Q. S.; Jin, Y.; Liao, L. S., Optimization of Low-Dimensional Components of Quasi-2d Perovskite Films for Deep-Blue Light-Emitting Diodes. *Adv. Mater.* **2019,** *31*, e1904319.

23. Jin, Y.; Wang, Z. K.; Yuan, S.; Wang, Q.; Qin, C.; Wang, K. L.; Dong, C.; Li, M.; Liu, Y.; Liao, L. S., Synergistic Effect of Dual Ligands on Stable Blue Quasi-2d Perovskite Light-Emitting Diodes. *Adv. Funct. Mater.* **2019**, 1908339.

24. Worku, M.; Tian, Y.; Zhou, C.; Lin, H.; Chaaban, M.; Xu, L.-j.; He, Q.; Beery, D.; Zhou, Y.; Lin, X., Hollow Metal Halide Perovskite Nanocrystals with Efficient Blue Emissions. *Sci Adv* **2020,** *6*, eaaz5961.

25. Yang, X.; Zhang, X.; Deng, J.; Chu, Z.; Jiang, Q.; Meng, J.; Wang, P.; Zhang, L.; Yin, Z.; You, J., Efficient Green Light-Emitting Diodes Based on Quasi-Two-Dimensional Composition and Phase Engineered Perovskite with Surface Passivation. *Nat Commun* **2018,** *9*, 570.

26. Jiang, Y.; Qin, C.; Cui, M.; He, T.; Liu, K.; Huang, Y.; Luo, M.; Zhang, L.; Xu, H.; Li, S., Spectra Stable Blue Perovskite Light-Emitting Diodes. *Nat Commun* **2019,** *10*, 1-9.

27. Liu, N.; Liu, P.; Zhou, H.; Bai, Y.; Chen, Q., Understanding the Defect Properties of Quasi-2d Halide Perovskites for Photovoltaic Applications. *The Journal of Physical Chemistry Letters* **2020,** *11*, 3521-3528.

28. Lee, S.; Park, J. H.; Lee, B. R.; Jung, E. D.; Yu, J. C.; Di Nuzzo, D.; Friend, R. H.; Song, M. H., Amine-Based Passivating Materials for Enhanced Optical Properties and Performance of Organic-Inorganic Perovskites in Light-Emitting Diodes. *J Phys Chem Lett* **2017,** *8*, 1784-1792.

29. Kerner, R. A.; Schloemer, T. H.; Schulz, P.; Berry, J. J.; Schwartz, J.; Sellinger, A.; Rand, B. P., Amine Additive Reactions Induced by the Soft Lewis Acidity of Pb 2+ in Halide Perovskites. Part I: Evidence for Pb–Alkylamide Formation. *J Mater Chem C* **2019,** *7*, 5251-5259.

30. Jurow, M. J.; Morgenstern, T.; Eisler, C.; Kang, J.; Penzo, E.; Do, M.; Engelmayer, M.; Osowiecki, W. T.; Bekenstein, Y.; Tassone, C., Manipulating the Transition Dipole Moment of Cspbbr3 Perovskite Nanocrystals for Superior Optical Properties. *Nano Lett.* **2019,** *19*, 2489-2496.
31. de Mello, J. C.; Wittmann, H. F.; Friend, R. H., An Improved Experimental Determination of External Photoluminescence Quantum Efficiency. *Adv. Mater.* **1997,** *9*, 230-232.
32. Halder, N.; Wagner, C., Separation of Particle Size and Lattice Strain in Integral Breadth Measurements. *Acta Crystallographica* **1966,** *20*, 312-313.
33. Kresse, G.; Furthmüller, J., Efficient Iterative Schemes for Ab Initio Total-Energy Calculations Using a Plane-Wave Basis Set. *Phys Rev B* **1996,** *54*, 11169.
34. Kresse, G.; Joubert, D., From Ultrasoft Pseudopotentials to the Projector Augmented-Wave Method. *Phys Rev B* **1999,** *59*, 1758.
35. Perdew, J. P.; Ruzsinszky, A.; Csonka, G. I.; Vydrov, O. A.; Scuseria, G. E.; Constantin, L. A.; Zhou, X.; Burke, K., Restoring the Density-Gradient Expansion for Exchange in Solids and Surfaces. *Phys. Rev. Lett.* **2008,** *100*, 136406.
36. Stoumpos, C. C.; Malliakas, C. D.; Peters, J. A.; Liu, Z.; Sebastian, M.; Im, J.; Chasapis, T. C.; Wibowo, A. C.; Chung, D. Y.; Freeman, A. J., Crystal Growth of the Perovskite Semiconductor Cspbbr3: A New Material for High-Energy Radiation Detection. *Cryst. Growth Des.* **2013,** *13*, 2722-2727.